Dyes and Pigments 133 (2016) 161–172

Contents lists available at ScienceDirect

Dyes and Pigments

journal homepage: www.elsevier.com/locate/dyepig

Alkyl chain length dependence of the charge-transfer, recombination and electron diffusion length on the photovoltaic performance in double donor-acceptor-based organic dyes for dye sensitized solar cells

Yong Hui Lee [a], Ramesh Kumar Chitumalla [b], Bo Youn Jang [a], Joonkyung Jang [b], Suresh Thogiti [a, *], Jae Hong Kim [a, **]

[a] Department of Chemical Engineering, Yeungnam University, 214-1, Dae-hakro 280, Gyeongsan, Gyeongbuk, 712-749, South Korea
[b] Department of Nanoenergy Engineering, Pusan National University, Busan, 609-735, South Korea

ARTICLE INFO

Article history:
Received 24 March 2016
Received in revised form
19 May 2016
Accepted 20 May 2016
Available online 1 June 2016

Keywords:
Dye-sensitized solar cell
Double donor-acceptor dyes
DFT study
Alkyl chain length
Diffusion length

ABSTRACT

A series of double donor-acceptor organic dyes (C4–C12) have been synthesized to investigate the influence of the alkyl chain length between the two chromophores on the performance of dye sensitized solar cells (DSSCs). The chain length dependent performance was investigated further using the electrochemical impedance and stepped light induced transient measurement methods. Dye with longer alkyl chain (C6–C12) shows a broader and higher IPCE as well as photo-current density (Jsc) with an enhanced photovoltage (Voc) relative to the reference PTZ-S. In contrast, C4 with shorter alkyl chain presents a relatively low IPCE within the whole spectral region, along with low Jsc and Voc, which predominately arising from the short electron diffusion length with significant electron loss during charge transport. The higher Jsc and Voc obtained with the devices incorporating C10 and C12 dyes with long alkyl chain resulted in a higher conversion efficiencies of 4.02% and 4.03%, respectively, (3.14% for single donor-acceptor dye PTZ-S). Density functional theory simulations were also performed to examine the effect of the alkyl chain length on electrochemical and optical properties of the dyes. Adsorption studies of the dyes on TiO_2 clusters were carried out to explain the variation in Jsc with the alkyl chain length.

© 2016 Elsevier Ltd. All rights reserved.

1. Introduction

In recent years, organic dyes have attracted considerable attention for use as sensitizers in dye sensitized solar cells (DSSCs) owing to their strong absorption in the visible region, as well as their optical, photo-physical and electrochemical properties, which can be tuned readily by peripheral substitutions [1–3]. The light-harvesting unit is a potent part of the dye sensitizer. Generally, the π-conjugated bridge structure with electron donor-acceptor (D-π-A) moieties is effective for intramolecular charge transfer. DSSCs with these dyes show better performance [1–17]. If the light-harvesting units of the D-π-A sensitizer increase, the photovoltaic performance of DSSCs should increase. Therefore, there has been considerable interest in the design and synthesis of novel double donor-acceptor dyes bridged with an alkyl spacer system, which show dark current suppression, and improved absorption properties in the visible light range. The phenothiazine unit is a fairly strong donor, and organic dyes based on this unit have been applied successfully in the DSSCs research field and shown quite promising efficiencies [18–30]. Derong Cao et al. reported novel phenothiazine-based double branched (DB) dyes that contained double symmetric and asymmetric D-π-A systems bridged with a fixed alkyl chain, and obtained increased conversion efficiencies of DSSCs compared to the corresponding single D-π-A dyes [18–20]. The same group reported the impact of the position isomer of the

* Corresponding author.
** Corresponding author.
E-mail addresses: iictsuresh@gmail.com, sureshyu@ynu.ac.kr (S. Thogiti), jaehkim@ynu.ac.kr (J.H. Kim).

http://dx.doi.org/10.1016/j.dyepig.2016.05.035
0143-7208/© 2016 Elsevier Ltd. All rights reserved.

linkage in DB organic dyes on the photovoltaic performance of DSSCs [21]. In 2015, they also examine the effects of the linkage location in DB organic dyes on the photovoltaic performance of DSSCs [23]. Recently, our group reported a novel DB dye with unsymmetrical anchoring groups and obtained higher efficiency as compared to those of cells sensitized with DB dyes with symmetrical anchoring groups [31].

Increasing the alkyl chain length is believed to reduce the charge recombination dynamics and increase the electron lifetime because the better surface protection would facilitate electron injection, leading to high overall conversion efficiency [32–42]. Qipeng Chai et al. reported that the alkyl chain length is crucial to the photovoltaic performance of cyclopentadithiophene-bridged sensitizers [43]. Why structural modification of the organic dyes can greatly influence the performance of the sensitizer based DSSCs is easy to understand [44–46]. Taking these points into consideration, a series of organic sensitizers with different alkyl chain spacers C4–C12 were designed to obtain greater insight into the impact on the photovoltaic performance of the solar cells under the conditions of introducing different alkyl chain spacers to the sensitizers that bear symmetric double donor-acceptor systems (Fig. 1). The bridged alkyl chain length of double branched dyes was expected to influence the surface coverage of the dyes on the TiO_2 films, affecting the performance of the device. The corresponding single branched dye PTZ-S was also synthesized for comparison (Fig. 1).

To determine the correlations between the device performance and the alkyl chain length, this study investigated the optical and electrochemical properties and the photovoltaic performance of the DSSCs based on these double donor-acceptor dyes bridged with different alkyl chain spacers. Density functional theory (DFT) and time dependent DFT (TDDFT) calculations were performed on five organic dyes. The experimental photophysical data were confirmed by the computational simulations. The variation of the excitation energies with respect to the alkyl chain length of the dyes was examined through TDDFT simulations. Moreover, the effects of the alkyl chain length on the solar cell performance was studied by electrochemical impedance (EIS) and the stepped light induced transient measurement (SLIM) technique. As the alkyl chain length was increased, the current density, open-circuit voltage and overall performance of DSSC increased due to the decreased recombination resistance and increased charge transport, diffusion length, and electron lifetime.

2. Experimental

2.1. Synthesis

The synthetic routes of C4–C12 are displayed in Scheme 1. The structures of the compounds were identified by ^{1}H NMR. The ^{1}H NMR spectra of the final product are shown in Supporting Information (ESI).

2.1.1. 10-Hexyl-10H-phenothiazine (1)

An oven dried, 250 mL round bottom flask (RBF) was charged with *N*,*N*-dimethylformamide (DMF) (100 mL), 1-bromohexane (10.7 g, 0.065 mol), and sodium hydride (1.8 g, 0.075 mol). Subsequently, a DMF solution of phenothiazine (10 g, 0.05 mol) was added to the mother solution, and the reaction mixture was maintained at room temperature for 10 h. After the reaction was complete, the solution was neutralized with a dilute HCl aqueous solution. The mixture was extracted with chloroform/water. The organic solution was then concentrated. The resulting crude oily product was purified by column chromatography on silica gel with hexane. The product was obtained as a colorless liquid. Yield: 11.2 g (79%). ^{1}H NMR (300 MHz, DMSO-d_6): δ (ppm) 7.20 (d, 2H), 7.14 (d, 2H), 6.99 (d, 2H), 6.91 (t, 2H), 3.84 (t, 2H), 1.67–1.60 (m, 2H), 1.41–1.27 (m, 2H), 1.23–1.19 (m, 4H), 0.86–0.80 (m, 3H).

2.1.2. 10-Hexyl-10H- phenothiazine-3-carbaldehyde (2)

An oven dried, 250 mL round bottom flask was charged with a solution of DMF (13.2 g, 0.18 mol) and 1,2-dichloroethane (20 mL). Subsequently, 10-hexyl-10H-phenothiazine, 1 (5.0 g, 0.017 mol) in 1,2-dichloroethane (20 mL) was added slowly to the mixture for 30 min $POCl_3$ (10.7 g, 0.07 mol) was then added drop wise over a 30 min period. The mixture was stirred for 10 h at 90 °C, and then poured into ice water (300 mL), neutralized with an aqueous solution of NaOH, and extracted three times with chloroform. The solvent was removed under reduced pressure. The resulting product was purified by column chromatography on silica gel with ethyl acetate/hexane (1:5 v/v). The product was obtained as a yellow solid. Yield: 2.7 g (51%). ^{1}H NMR (300 MHz, $CDCl_3$): δ (ppm) 9.79 (s, 1H), 7.63 (d, 1H), 7.58 (s, 1H), 7.17 (d, 1H), 7.11 (d, 1H), 6.97 (d, 1H), 6.92 (d, 1H), 6.88 (d, 1H), 3.88 (t, 2H), 1.85–1.76 (m, 2H), 1.43–1.30 (m, 6H), 0.87 (m, 3H).

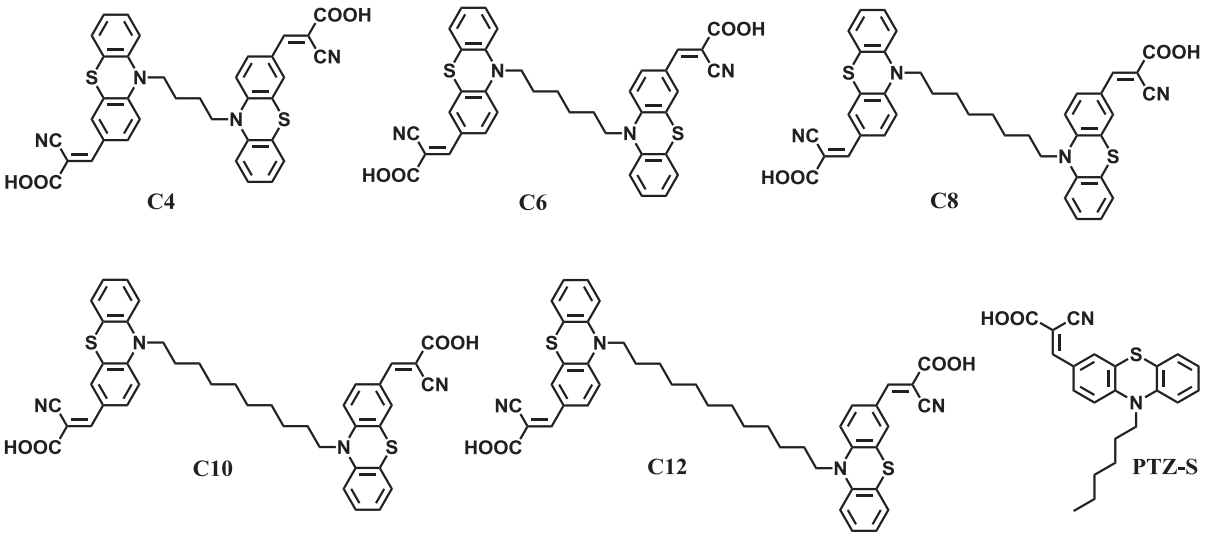

Fig. 1. Chemical structures of the new sensitizers C4–C12 and reference sensitizer PTZ-S.

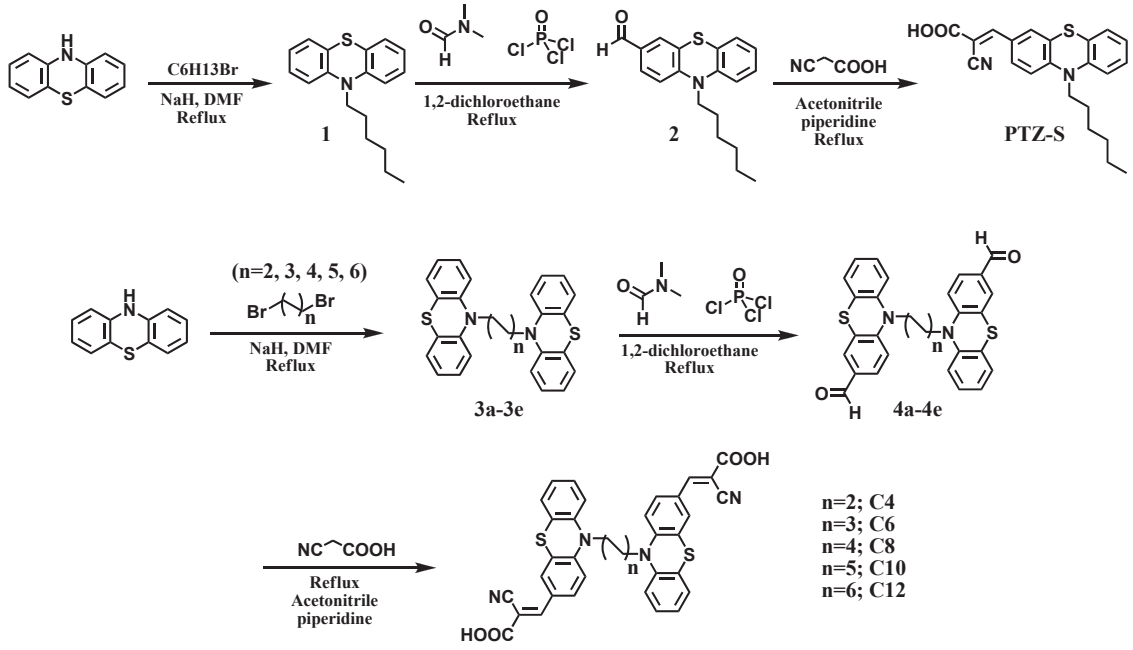

Scheme 1. Synthesis of dyes C4–C12 and reference PTZ-S.

2.1.3. 2-Cyano-3-(10-hexyl-10H-phenothiazine-3-yl)acrylic acid (PTZ-S)

In a dried, 100 mL round bottom flask, 10-hexyl-10H-phenothiazine-3-carbaldehyde, 2 (2.0 g, 6.4 mmol), 2-cyanoacetic acid (0.71 g, 8.3 mmol), and piperidine (0.081 g, 0.96 mmol) were dissolved in acetonitrile (10 mL). The reaction mixture was efluxed for 6 h. After cooling to room temperature, 5 mL of 2 M aqueous HCl was added and the mixture was stirred for 30 min. Then the mixture was washed with water and extracted three times with chloroform. The combined organic fractions were washed with brine and dried over Na_2SO_4. The solvent was removed under reduced pressure and the residue was purified by recrystallization in acetonitrile. The product was obtained as a black solid. Yield: 1.9 g (42%). ^{1}H NMR (300 MHz, $CDCl_3$): δ (ppm) 8.09 (s, 1H), 7.91 (d, 1H), 7.68 (s, 1H), 7.17 (d, 1H), 7.09 (d, 1H), 6.96 (d, 1H), 6.87 (d, 2H), 3.88 (t, 2H), 1.80 (d, 2H), 1.44–1.31 (m, 6H), 0.88 (m, 3H).

2.1.4. 1,4-Di (10H-phenothiazin-10-yl) butane (3a)

A 250 mL 3-neck flask was charged with 10H-phenothiazine (8.99 g, 45.1 mmol), and 1,4-dibromobutane (5 g, 20.5 mmol), NaH (4.1 g, 102.5 mmol) and 100 mL of DMF. The resulting mixture was stirred for 3 h at room temperature. The reaction mixture was then quenched with water and extracted three times with chloroform. The solvent was removed under reduced pressure and the product was purified by column chromatography on silica gel. Isolated yield = 74%. ^{1}H NMR (300 MHz, DMSO-d_6): δ (ppm) 7.15–7.10 (d, 8H), 6.96–6.89 (m, 8H), 3.88 (t, 4H), 1.82 (m, 4H).

2.1.5. 10,10′-(Butane-1,4-diyl)bis(10H-phenothiazine-3-carbaldehyde) (4a)

A 250 mL 3-neck flask was charged with 1,4-di(10H-phenothiazine-10-yl)butane (2 g, 4.40 mmol), and DMF (6.43 g, 88.0 mmol), $POCl_3$ (13.5 g, 88.0 mmol), and 20 mL of 1,2-dichloroethane. The resulting mixture was stirred for 2 h at 90–95 °C. The reaction mixture was quenched with water and extracted three times with chloroform. The solvent was removed under reduced pressure and the residue was purified by column chromatography using silica gel and ethyl acetate/hexane (1/3; v/v) as the eluent to give 10,10′-(butane-1,4-diyl)bis(10H-phenothiazine-3-carbaldehyde) as a yellow viscous liquid. Isolated yield = 90%. ^{1}H NMR (300 MHz, DMSO-d_6): δ (ppm) 9.78 (s, 2H), 7.66–7.64 (d, 2H), 7.53 (s, 2H), 7.16–7.09 (m, 6H), 7.04–6.98 (m, 4H), 3.98 (t, 4H), 1.84 (m, 4H).

2.1.6. (2E,2′E)-3,3′-(10,10′-(butane-1,4-diyl)bis(10H-phenothiazine-10,3-diyl)bis(2-cyanoacrylic acid) (C4)

A 100 mL 3-neck flask was charged with 10,10′-(butane-1,4-diyl) bis(10H-phenothiazine-3-carbaldehyde) (0.3 g, 0.59 mmol), 2-cyanoacetic acid (0.014 g, 0.16 mmol), piperidine (0.143 g, 1.68 mmol) and 10 mL of acetonitrile. The reaction mixture was refluxed for 6 h. After cooling to room temperature, 5 mL of 2 M aqueous HCl was added and the mixture was stirred for 30 min. Then the mixture was washed with water and extracted three times with chloroform. The combined organic fractions were washed with brine and dried over Na_2SO_4. The solvent was removed under reduced pressure and the residue was purified by recrystallization in acetone and methanol. The product was obtained as a black solid. Isolated yield = 90%. ^{1}H NMR (300 MHz, DMSO-d_6): δ (ppm) 8.11 (s, 2H), 7.87–7.84 (d, 2H), 7.74 (s, 2H), 7.19–7.09 (m, 6H), 7.05–6.96 (m, 4H), 3.98 (t, 4H), 1.84 (t, 4H).

2.1.7. 1,6-di(10H-phenothiazine-10-yl)hexane (3b)

A 250 mL 3-neck flask was charged with 10H-phenothiazine(8.99 g, 45.1 mmol), and 1,6-dibromohexane (5 g, 20.5 mmol), NaH (4.1 g, 102.5 mmol) and 100 mL of DMF. The synthetic method was similar to that used to synthesize compound 3a, and compound 3b was obtained in 74% yield. ^{1}H NMR (300 MHz, DMSO-d_6): δ (ppm) 7.20–7.10 (m, 8H), 6.97–6.90 (m, 8H), 3.81 (t, 4H), 1.64 (m, 4H), 1.39 (m, 4H).

2.1.8. 10,10′-(hexane-1,6-diyl)bis(10H-phenothiazine-3-carbaldehyde) (4b)

A 250 mL 3-neck flask was charged with 1,6-di(10H-phenothiazine-10-yl)hexane (2 g, 4.16 mmol), DMF (3.041 g, 41.6 mmol), $POCl_3$ (6.38 g, 41.6 mmol), and 10 mL of 1,2-dichloroethane. The synthetic method was similar to that used to synthesize compound 4a, and compound 4b was obtained as a yellow viscous liquid in

50% yield. ^{1}H NMR (300 MHz, DMSO-d_6): δ (ppm) 9.78 (s, 2H), 7.71–7.68 (d, 2H), 7.57 (s, 2H), 7.23–7.10 (m, 6H), 7.05–6.97 (m, 4H), 3.91 (t, 4H), 1.66 (m, 4H), 1.40 (m, 4H).

2.1.9. (2E,2′E)-3,3′-(10,10′-(hexane-1,6-diyl)bis(10H-phenothiazine-10,3-diyl)bis(2-cyanoacrylic acid) (C6)

A 100 mL 3-neck flask was charged with 10,10′-(hexane-1,6-diyl)bis(10H-phenothiazine-3-carbaldehyde) (0.5 g, 0.745 mmol), 2-cyanoacetic acid (0.19 g, 2.24 mmol), piperidine (0.019 g, 0.22 mmol), and 10 mL of acetonitrile. The synthetic method was similar to that used to synthesize compound C4, and compound C6 was obtained as a black solid in 60% yield. ^{1}H NMR (300 MHz, DMSO-d_6): δ (ppm) 8.20 (s, 2H), 7.96–7.93 (d, 2H), 7.84–7.83 (s, 2H), 7.30–7.20 (m, 6H), 7.11–7.03 (m, 4H), 3.97 (t, 4H), 1.73 (m, 4H), 1.48 (m, 4H).

2.1.10. 1,8-di(10H-phenothiazine-10-yl)octane (3c)

A 250 mL 3-neck flask was charged 10H-phenothiazine (8.07 g, 40.5 mmol), and 1,8-dibromo octane (5 g, 18.4 mmol), NaH (4.42 g, 110.4 mmol) and 100 mL of DMF. The synthetic method was similar to that used to synthesize compound 3a, and compound 3c was obtained in 75% yield. ^{1}H NMR (300 MHz, DMSO-d_6): δ (ppm) 7.21–7.11 (m, 8H), 7.0–6.92 (m, 8H), 3.85 (t, 4H), 1.55 (m, 4H), 1.25 (m, 8H).

2.1.11. 10,10′-(octane-1,8-diyl)bis(10H-phenothiazine-3-carbaldehyde) (4c)

A 250 mL 3-neck flask was charged with 1,8-di(10H-phenothiazine-10-yl)octane (2 g, 3.54 mmol), DMF (5.19 g, 71.0 mmol), $POCl_3$ (10.9 g, 71.0 mmol), and 20 mL of 1,2-dichloroethane. The synthetic method was similar to that used to synthesize compound 4a, and compound 4c was obtained as a viscous yellow liquid in 50% yield. ^{1}H NMR (300 MHz, DMSO-d_6): δ (ppm) 9.79 (d, 2H), 7.72–7.70 (d, 2H), 7.58 (s, 2H), 7.24–7.13 (m, 6H), 7.07–6.97 (m, 4H), 3.91 (t, 4H), 1.64 (m, 4H), 1.34 (m, 8H).

2.1.12. (2E,2′E)-3,3′-(10,10′-(octane-1,8-diyl)bis(10H-phenothiazine-10,3-diyl)bis(2-cyanoacrylic acid) (C8)

A 100 mL 3-neck flask was charged with 10,10′-(octane-1,8-diyl) bis(10H-phenothiazine-3-carbaldehyde) (0.5 g, 0.715 mmol), 2-cyanoacetic acid (0.182 g, 2.15 mmol), piperidine (0.018 g, 0.21 mmol), and 10 mL of acetonitrile. The synthetic method was similar to that used to synthesize compound C4, and compound C8 was obtained as a black solid in 60% yield. ^{1}H NMR (300 MHz, DMSO-d_6): δ (ppm) 8.14 (s, 2H), 7.92–7.24 (d, 4H), 7.23–7.12 (m, 10H), 3.91 (t, 4H), 1.65 (m, 4H), 1.25 (m, 8H).

2.1.13. 1,10-di(10H-phenothiazine-10-yl)decane (3d)

A 250 mL 3-neck flask was charged with 10H-phenothiazine (7.45 g, 37.4 mmol), 1,10-dibromodecane (5 g, 17.0 mmol), NaH (4.08 g, 102.0 mmol), and 100 mL of DMF. The synthetic method was similar to that used to synthesize compound 3a, and compound 3d was obtained in 75% yield. ^{1}H NMR (300 MHz, DMSO-d_6): δ (ppm) 7.20–7.7.10 (m, 8H), 7.00–6.89 (m, 8H), 3.83 (t, 4H), 1.63 (m, 4H), 1.32 (m, 4H), 1.15 (m, 8H).

2.1.14. 10,10′-(decane-1,10-diyl)bis(10H-phenothiazine-3-carbaldehyde) (4d)

A 250 mL 3-neck flask was charged with 1,10-di(10H-phenothiazine-10-yl)decane (2 g, 3.40 mmol), DMF (4.97 g, 68.0 mmol), $POCl_3$ (10.43 g, 68.0 mmol), and 20 mL of 1,2-dichloroethane. The synthetic method was similar to that used to synthesize compound 4a, and compound 4d was obtained as a yellow viscous liquid in 50% yield. ^{1}H NMR (300 MHz, DMSO-d_6): δ (ppm) 9.78 (s, 2H), 7.72–7.69 (d, 2H), 7.58 (s, 2H), 7.24–7.13 (m, 6H), 7.07–6.96 (m, 4H), 3.92 (t, 4H), 1.65 (m, 4H), 1.33–1.15 (m, 12H).

2.1.15. (2E,2′E)-3,3′-(10,10′-(decane-1,10-diyl)bis(10H-phenothiazine-10,3-diyl)bis(2-cyanoacrylic acid) (C10)

A 100 mL 3-neck flask was charged with 10,10′-(decane-1,10-diyl)bis(10H-phenothiazine-3-carbaldehyde) (0.5 g, 0.69 mmol), 2-cyanoacetic acid (0.176 g, 2.07 mmol), piperidine (0.018 g, 0.207 mmol), and 10 mL of acetonitrile. The synthetic method was similar to that used to synthesize compound C4, and compound C10 was obtained as a black solid in 60% yield. ^{1}H NMR (300 MHz, DMSO-d_6): δ (ppm) 8.15 (s, 2H), 7.92–7.90 (d, 2H), 7.80 (s, 2H), 7.24–7.14 (m, 6H), 7.08–6.98 (m, 4H), 3.93 (t, 4H), 1.66 (m, 4H), 1.18 (m, 12H).

2.1.16. 1,12-di(10H-phenothiazine-10-yl)dodecane (3e)

A 250 mL 3-neck flask was charged with 10H-phenothiazine (6.68 g, 33.5 mmol), and 1,12-dibromododecane (5 g, 15.2 mmol), NaH (3.65 g, 91.2 mmol), and 100 mL of DMF. The synthetic method was similar to that used to synthesize compound 3a, and compound 3e was obtained in 90% yield. ^{1}H NMR (300 MHz, DMSO-d_6): δ (ppm) 7.21–7.11 (m, 8H), 7.00–6.89 (m, 8H), 3. 85 (t, 4H), 1.66 (m, 4H), 1.35 (m, 4H), 1.14 (m, 12H).

2.1.17. 10,10′-(dodecane-1,12-diyl)bis(10H-phenothiazine-3-carbaldehyde) (4e)

A 250 mL 3-neck flask was charged with 1,12-di(10H-phenothiazine-10-yl)dodecane (0.5 g, 0.89 mmol), DMF (1.3 g, 17.8 mmol), $POCl_3$ (2.73 g, 17.8 mmol), and 20 mL of 1,2-dichloroethane. The synthetic method was similar to that used to synthesize compound 4a, and compound 4e was obtained as a yellow viscous liquid in 50% yield. ^{1}H NMR (300 MHz, DMSO-d_6): δ (ppm) 9.78 (s, 2H), 7.72–7.69 (d, 2H), 7.56 (s, 2H), 7.24–7.13 (m, 6H), 7.07–6.96 (m, 4H), 3.92 (t, 4H), 1.65 (m, 4H), 1.33–1.15 (m, 16H).

2.1.18. (2E,2′E)-3,3′-(10,10′-(dodecane-1,12-diyl)bis(10H-phenothiazine-10,3-diyl)bis(2-cyanoacrylic acid) (C12)

A 100 mL 3-neck flask was charged with 10,10′-(dodecane-1,12-diyl)bis(10H-phenothiazine-3-carbaldehyde) (0.3 g, 0.483 mmol), 2-cyanoacetic acid (0.123 g, 1.45 mmol), piperidine (0.012 g, 0.14 mmol), and 10 mL of acetonitrile. The synthetic method was similar to that used to synthesize compound C4, and compound C12 was obtained as a black solid in 60% yield. ^{1}H NMR (300 MHz, DMSO-d_6): δ (ppm) 8.15 (s, 2H), 7.93–7.90 (m, 2H), 7.82 (s, 2H), 7.25–7.14 (m, 6H), 7.09–6.97 (m, 4H), 3. 94 (t, 4H), 1.68 (m, 4H), 1.37 (m, 4H), 1.15 (m, 12H).

2.2. Material and instruments

All starting materials and solvents were purchased from Sigma-Aldrich and used as received. The ^{1}H NMR spectra were recorded on a Bruker Advance NMR 300 MHz spectrometer. The UV–Vis spectra were recorded using Cary 5000 UV–Vis–NIR Spectrophotometer.

2.3. Computational details

All ground state and excited state simulations were performed using the Gaussian 09 [47] quantum chemical program. Geometry optimization and vibrational frequency analysis of all the dyes were carried out at the B3LYP/6-31G(d) level of theory [48–50]. The theoretical singlet equilibrium structures were obtained when the maximum internal forces acting on all the atoms and the stress were less than 4.5×10^{-4} eV/Å and 1.01×10^{-3} kbar, respectively. The minima were confirmed by harmonic vibrational frequency analysis by ensuring all positive frequencies. The UV–visible absorption spectra were simulated with the pre optimized structures

using the TDDFT formalism at the CAM-B3LYP/6-31G(d) level of theory [51]. In the TDDFT simulations, 25 vertical singlet excitations were calculated to obtain the UV–vis absorption spectra of the dyes. The experimental acetonitrile solution was mimicked using the polarizable continuum model [52,53] in the TDDFT simulations.

2.4. Solar cell fabrication and characterization

The fluorine-doped tin oxide (FTO) transparent conducting glasses (Pilkington, 15 Ω/cm^2) were cleaned with methanol, D.I water and acetone. The cleaned FTO glasses (Pilkington, 15 Ω/cm^2) were coated with transparent TiO_2 pastes (20–30 nm in diameter, Dyesol Ltd.) using the doctor blade technique, followed by sintering at 450 °C for 30 min. The TiO_2 particle scattering layer (200 nm in diameter, Dyesol Ltd.) was deposited on the transparent nano-porous TiO_2 films, followed by sintering at 450 °C for 30 min. Two layers of TiO_2 films were treated with a 40 mM of a $TiCl_4$ aqueous solution at 70 °C for 30 min and then sintered at 450 °C for 30 min. After cooling to 100 °C, the TiO_2 films were immersed in 0.3 mM dye solutions at 25 °C for 24 h in the dark and the residual dye was rinsed off with acetonitrile to provide the working electrode. The platinum paste was deposited on the FTO glasses using the doctor blade technique, followed by sintering at 450 °C for 30 min to give the counter electrodes. The working electrode and Pt counter electrodes were assembled into a sealed sandwich cell with a 60 μm thick Surlyn film (Dupont), which was then filled with an electrolyte solution through pre-drilled holes on the Pt counter electrode. The electrolyte solution contained 1-butyl-3-methylimidazolium iodide (0.7 M), lithium iodide (LiI, 0.2 M), iodine (I_2, 0.05 M), and *t*-butylpyridine (TBP, 0.5 M) in acetonitrile/valeronitrile (85:15, v/v).

2.5. Photovoltaic characterization

The photo current density-voltage (J-V) characteristics of the prepared DSSCs were measured under AM 1.5 irradiation with an incident power of 100 mW/cm^2 (PEC-L11, Peccell Technologies, Inc.). The incident monochromatic photon-to-current efficiencies (IPCEs) were recorded as a function of the light wavelength using an IPCE measurement instrument (PEC-S20, Peccell Technologies, Inc.). Electrochemical impedance spectroscopy (EIS) was carried out using a computer-controlled potentiostat (IVIUMSTAT, IVIUM) at the open circuit voltage with a 10 mV of amplitude and an AC frequency range between 100 kHz and 0.1 Hz (PEC-L11, Peccell Technologies, Inc.). The electron diffusion coefficient and electron lifetime of the DSSCs were measured using the stepped light-induced transient measurements of the photocurrent and voltage (SLIM-PCV) using a diode laser (Helium–Neon laser power supply, Thor Lab, λ = 632.8 nm). The current transient was monitored using a digital phosphor oscilloscope (Tektronic DPO 4102B-L) through a current amplifier.

3. Results and discussion

Fig. 2a presents the UV–Vis absorption spectra of the double donor-acceptor dyes, C4–C12, and single donor-acceptor dye, PTZ-S, dissolved in DMF. Table 1 shows that the peak positions are similar for all dyes. All the dyes exhibited absorption maxima at 396–402 nm, which might be due to intramolecular charge transfer between the phenothiazine donor and terminal cyano-acetic acid acceptor. The absorption bands observed for these di-anchoring dyes C4–C12 are similar to that observed for the corresponding mono-anchoring dye, PTZ-S (Fig. 2a). Despite this drawback, the molar extinction coefficients (ε) of the di-anchoring dyes were higher than that of the mono-anchoring dye PTZ-S.

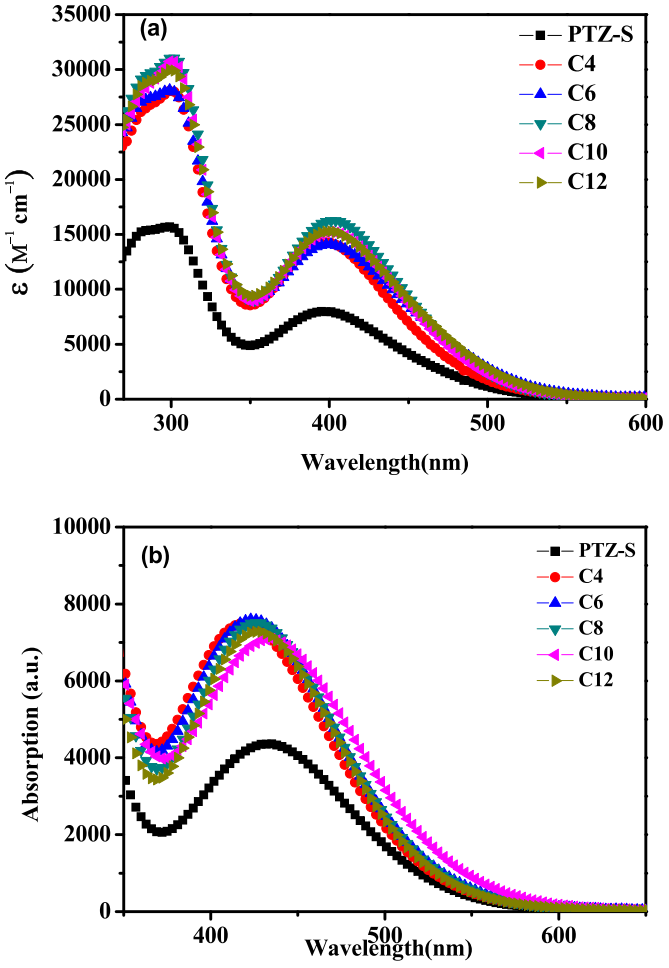

Fig. 2. Absorption spectra of the dyes (a) in DMF solution; (b) anchored on the TiO_2 films.

Fig. 2b shows the absorption spectra of these dyes anchored on a TiO_2 film. The spectra were slightly different for C4–C12 with absorption maxima ranging from 419 to 433 nm. Compared to the absorption spectra in solution, a bathochromic shift (23–33 nm) was observed for the C4–C12-dyes upon adsorption on TiO_2 from a DMF solution. This bathochromic shift has been observed for many organic dyes and can be attributed mainly to the formation of J-type aggregation. In particular, the C10 and C12 dyes exhibited a red shifted pattern (33 and 25 nm) compared to the other dyes, which benefits the capture of photons over an extended region.

Fig. 3 shows the optimized ground state geometries of the dyes, C4 and C6, whereas the geometries of the dyes, C8, C10, and C12, are given in the supporting information (Fig. S1). The geometry of the phenothiazine part in each dye was not precisely planar but slightly bent in the middle with a butterfly shape. The non-planar geometry of the phenothiazine ring can help reduce the aggregation effect of the dyes on the TiO_2 surface. The distance between two phenothiazine rings is also given along with the optimized geometries. The increase in the distance between the two phenothiazine rings is approximately 2.55 Å with each $-CH_2-CH_2-$ addition. The dipole moment of the dye increased gradually with increasing alkyl chain length, reaching a maximum for dye C12.

Fig. 4 presents the electron density distribution in the frontier molecular orbitals of all the dyes. The electron density in the highest occupied molecular orbitals (HOMOs) of all the dyes was localized over one phenothiazine ring and partly on the anchoring

Table 1
Optical and photovoltaic parameters of the DSSCs.

Dye	λ_{max}		Dye amount (10^{-4} mol/cm^2)	Jsc (mA/cm^2)	Voc (V)	FF	η
	Sol. (ε; M^{-1}cm^{-1})	Film					
N719				14.363	0.760	0.68	7.17
PTZ-S	396 (7968)	432	3.67	6.575	0.670	0.70	3.14
C4	396 (14,353)	417	2.57	6.133	0.670	0.72	2.84
C6	399 (14,089)	423	2.57	7.804	0.670	0.71	3.60
C8	402 (16,332)	425	2.41	8.713	0.695	0.68	4.00
C10	402 (15,276)	434	2.35	8.817	0.695	0.68	4.03
C12	400 (15,276)	427	2.21	8.754	0.705	0.68	4.02

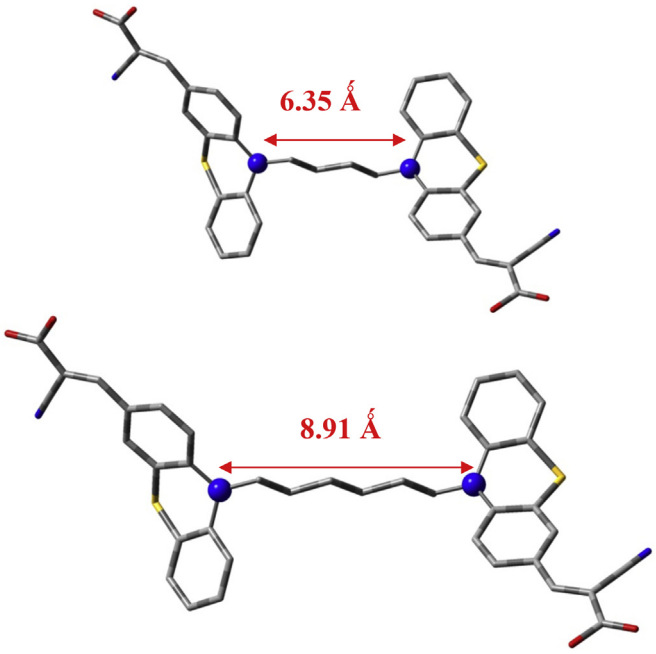

Fig. 3. Ground state optimized geometries of C4 (top) and C6 (bottom) dyes obtained at the B3LYP/6-31G(d) level of theory. The hydrogen atoms are omitted for clarity.

group. The electron density was shifted to the other phenothiazine ring in the lowest unoccupied molecular orbitals (LUMOs) of the dyes. In the LUMOs, the electron density was localized more towards the anchoring group rather than the phenothiazine moiety.

The HOMO energies (oxidation potential) of the dyes helps, to some extent, evaluate thermodynamically the possibility of dye regeneration. The HOMO eigenvalues of all the dyes (Table 2) were just below −5.30 eV, and were also lower in energy than the redox potential (−5.20 eV) of the I^-/I_3^- redox couple, which facilitates effective dye regeneration from its oxidized state. From the values, there was little variation in the HOMO energies when changing from C4 to C8, and the energy values almost converged when changing from C8 to C12. The LUMO energy of the dye C4 was −2.51 eV, and very small stabilization in LUMO energies from C4 to C12 (Table 2). The LUMO energies were sufficiently above the conduction band (−4.20 eV) of TiO_2. The high LUMO energy level of all the dyes can provide an adequate driving force for electron injection to the conduction band of the TiO_2 from the dye excited state.

Table 2
Calculated eigenvalues of the various molecular orbitals of the dyes along with the HOMO-LUMO energy gaps obtained at the B3LYP/6-31G(d) level of theory.

Dye	HOMO-1	HOMO	LUMO	LUMO+1	$\Delta_{HOMO-LUMO}$
C4	−5.51	−5.34	−2.51	−2.49	2.83
C6	−5.48	−5.32	−2.50	−2.48	2.82
C8	−5.47	−5.32	−2.50	−2.48	2.82
C10	−5.46	−5.31	−2.49	−2.48	2.82
C12	−5.46	−5.31	−2.49	−2.48	2.82

The experimentally obtained optical properties of the dyes were also well supported by computational studies using TDDFT formalism. The absorption maxima of the dyes obtained in the low energy region were in excellent agreement with the corresponding experimental data. The simulated absorption maxima of the dyes were approximately 405 nm with small variations with changing from the C4 dye to the C12 dye. The optical transitions of these five dyes were transferred mainly from the HOMO to LUMO+1. The UV−visible absorption data showed that there is a decrease in the excitation energies (eV) from dye C4 to C6 and C6 to C8. The excitation energies almost converged by varying from dye C8 to C12 (Fig. 5). These lower and converged excitation energies of dyes C8, C10, and C12 may be responsible for showing higher and similar efficiencies over dyes C4 and C6. Although the observed variation in the excitation energies with increasing alkyl chain length is consistent with the experimentally observed trend, the variation is not significant to explain the variation of their respective DSSC efficiencies. In addition, to explain the effect of alkyl chain length on the overall efficiency, adsorption studies of the five dyes on the TiO_2 (101) cluster were carried out.

Fig. 6 shows the electron density distribution in the systems, C4@TiO_2 and C6@TiO_2, whereas those of the other dyes are shown in the supporting information (Fig. S2). The electron density distribution in the HOMOs and LUMOs of these five dye@TiO_2 systems showed no reasonable deviation. In the case of HOMOs, despite the presence of two phenothiazine rings, the electron density was localized mainly over one phenothiazine ring attached directly to the TiO_2 cluster through the anchoring group. On the other hand, in the case of the LUMOs, the electron density was shifted completely to the TiO_2 cluster. The shifting of the electron density from the dye to the TiO_2 indicates the direct electron injection process from the excited state of the dye to the conduction band of TiO_2.

As the electronic coupling between the excited state of the dye and the unoccupied states of TiO_2 has a direct effect on the overall efficiency of the DSSC, the interaction between the dye sensitizer and the TiO_2 is a very prominent aspect. Therefore, adsorption studies of the dyes on TiO_2 cluster were performed to evaluate the effect of the alkyl chain length on the efficiency of the DSSCs. Calculation of the binding energy between the dye and TiO_2 proceeds by tethering one of the anchoring groups of the dye to a clean and relaxed anatase $(TiO_2)_{16}$ cluster in an appropriate bidentate bridging motif. The binding energies were then obtained by subtracting the energy of the total system from the sum of the energies of the dye and TiO_2:

$$E_{BE} = (E_{Dye} + E_{Tio_2}) - E_{Dye@Tio_2}$$

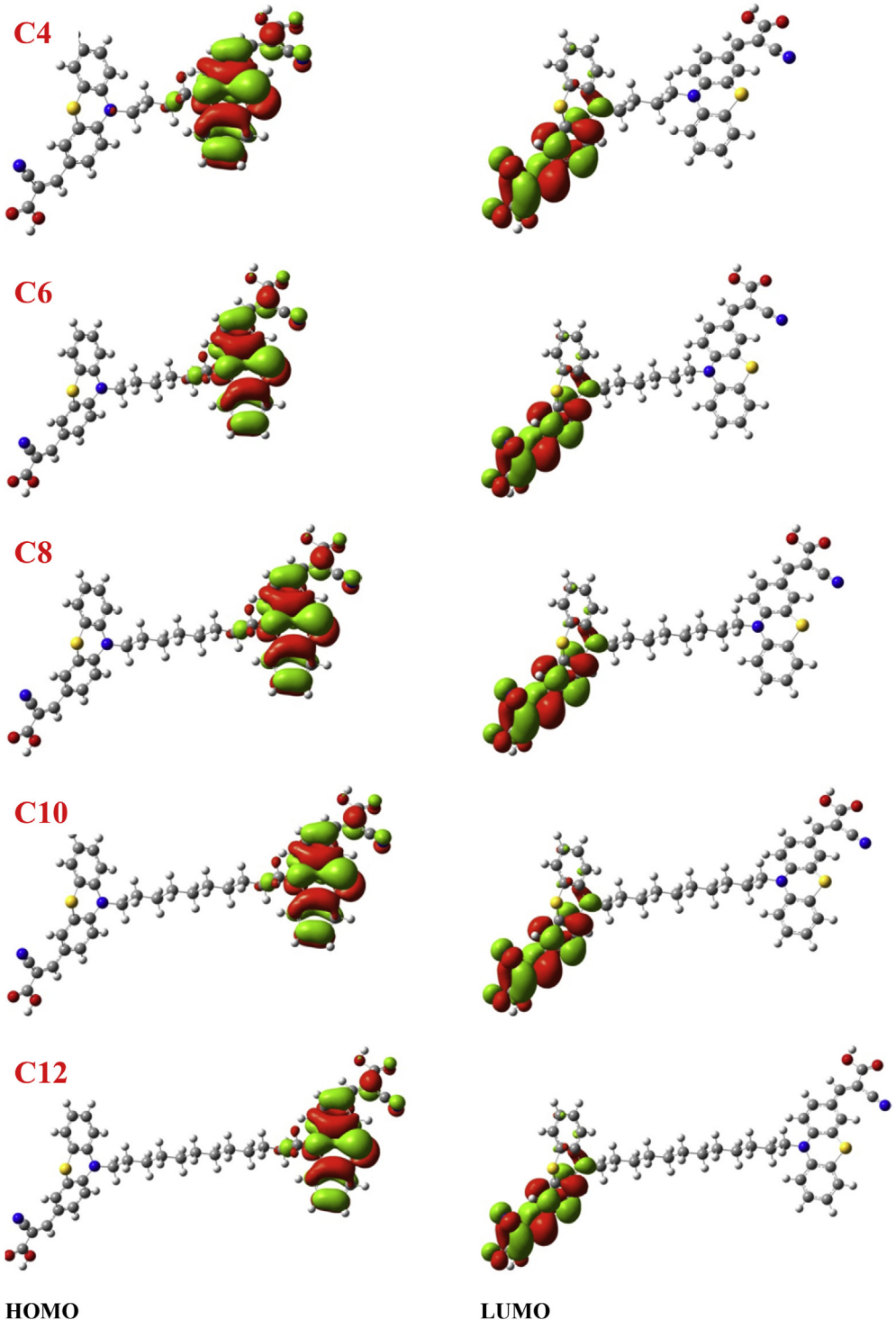

Fig. 4. Electron density distribution in the frontier molecular orbitals of dyes C4–C12 obtained at the B3LYP/6-31G(d) level of the theory. (Isosurface: ±0.02 e Å^{-3}).

Here, a positive E_{BE} value indicates stable adsorption. The binding energies obtained in this way were then plotted as a function of the alkyl chain length (Fig. 7). The dyes, C4 and C6, showed relatively lower binding energies compared to those of C8 to C12. The dyes, C8, C10, and C12, showed similar binding energies with small deviations, which leads to similar Jsc and overall efficiencies.

The current density–voltage (J–V) properties of the DSSCs based on these double donor-acceptor dyes were evaluated under standard AM 1.5G illumination and compared with that of the corresponding single donor-acceptor dye (PTZ-S) and conventional ruthenium dye sensitizer (N719). Fig. 8 and Table 1 present the J–V curves and photovoltaic parameters. The short-circuit current density (Jsc) and open-circuit voltage (Voc) increase gradually with increasing alkyl chain length. This leads to a linear increase in the device efficiency with increasing chain length (Fig. 8). All the

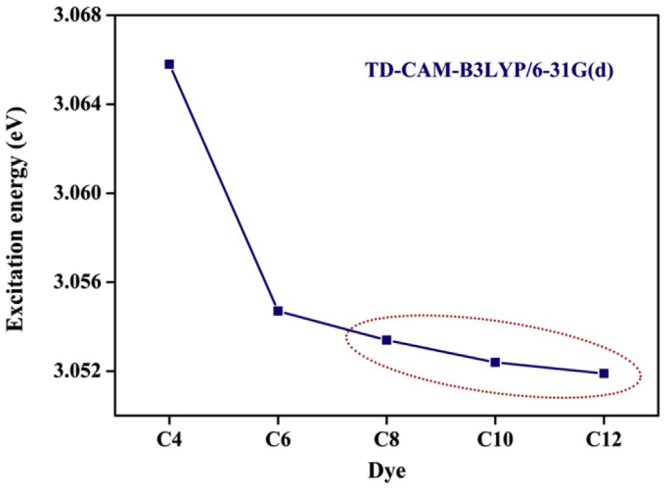

Fig. 5. Variation in the excitation energies with the alkyl chain length obtained at the CAM-B3LYP/6-31G(d) level of theory.

double donor-acceptor dyes showed improved performance compared to the single donor-acceptor dye. For the shortest chain (C4), however, a decrease in short-circuit current density and cell efficiency was observed.

As is well known, the presence of long alkyl chains in the dye sensitizer could increase the device efficiency due to a decrease in charge recombination [32–42]. Other groups have reported that the surface potential of the sensitizer increases with increasing alkyl chain length and could be attributed to the increase in photovoltage (Voc) [54,55]. The adsorption amount was measured further to shed light on the possible interactions. The adsorption amount of the C4–C12 dyes was in the order C4 ≥ C6 > C8 > C10 > C12 (Table 1). With respect to the dyes with long alkyl chain, the decreased alkyl chain length in the dyes with a short alkyl chain leads to more void space between the electrolyte and the TiO_2 films, which may facilitate the recombination of injected electrons and redox species. In these dyes, although the adsorbed amount of dye decreased with increasing alkyl chain length, the dye with the long alkyl chain bridge is expected to

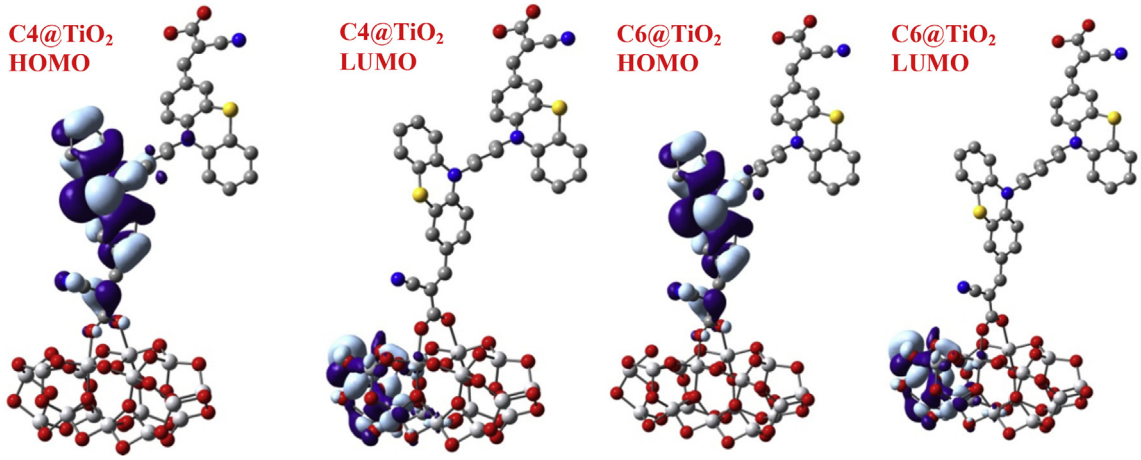

Fig. 6. Computed isodensity (isodensity contour: 0.02 e $Å^{-3}$) surface plots for the frontier molecular orbitals of C4@TiO_2 and C6@TiO_2 obtained at the B3LYP/6-31G(d) level of theory.

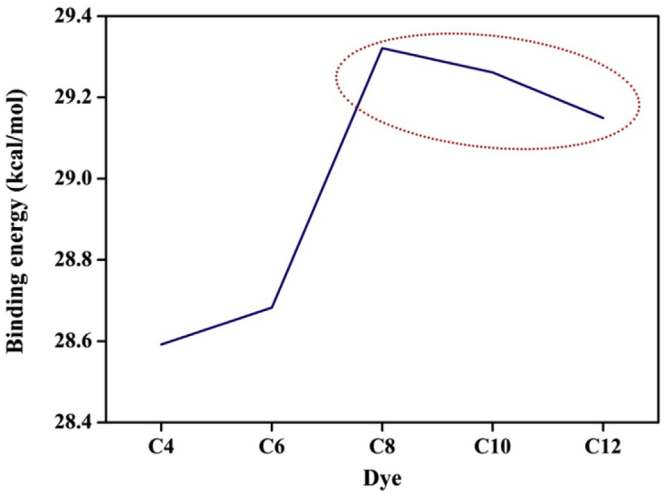

Fig. 7. Variation in binding energies of the dyes with the TiO_2 (101) cluster.

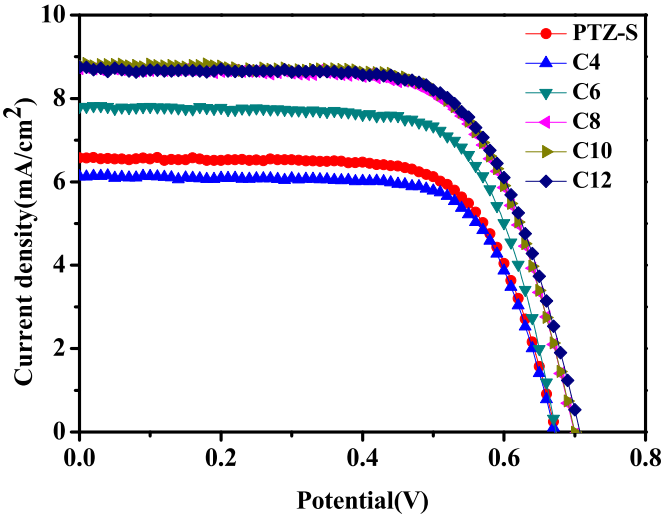

Fig. 8. J-V curves of the DSSCs sensitized with C4–C12 and PTZ-S.

provide a more protected area. The longer alkyl chain between two chromophores is believed to facilitate greater protection and have a high propensity to prevent the binding of the iodide–triiodide redox couple (Fig. 9), which may form a compact layer to effectively retard the charge recombination process and improve the short circuit current density and open-circuit voltage.

Fig. 10 compares the incident photon to current efficiency (IPCE) spectra for the DSSCs sensitized with C4–C12 with those of the N719 and PTZ-S sensitized DSSC. With the exception of the C4-based device, all the dyes exhibited improved IPCE values compared to the single donor-acceptor dye. The IPCE is a product of the electron injection efficiency (Φ_{inj}), light-harvesting efficiency (LHE) and charge collection efficiency (η_c) [56]. The relative low IPCE value for C4 dye is probably due to the low electron injection efficiency or charge collection efficiency. The charge collection efficiency of the excited C4 dye is insufficient, as revealed by the SLIM-PCV (discussed in following section). Therefore, the electron injection efficiency or the charge collection efficiency is can be reduced dramatically, which lowers the IPCE significantly under similar adsorption conditions. The narrow spectral window and lower IPCE values for the shorter alkyl chain reflects the lower photocurrent and the lower photovoltaic performance. Fig. 10 shows that the IPCE response in the visible region increases with increasing alkyl chain length for the C4–C12 sensitized devices, which is in agreement with the trend for the Jsc for C4–C12 described above.

EIS was employed under illumination and dark conditions to evaluate the interfacial charge-transfer/recombination processes in the DSSCs containing these dyes. Fig. 11 shows the Nyquist plots; the high-frequency region represents the series resistance (R1), corresponding to the diameter of the first semicircle; the larger semicircle in the mid-frequency region reflects the charge transfer/recombination resistance (R3) at the TiO_2/dye/electrolyte interface. As shown in Table 3, there was little difference in the R2 values because the same counter electrode (Pt) and electrolyte was used. On the other hand, there was a substantial difference in the R3 values, which indicates that the charge-transfer behavior between TiO_2 and the electrolyte is altered significantly, which is due likely to surface modification with different alkyl chain length dyes. R3 values of 24.91, 19.48, 17.38, 17.30, and 16.37 Ω were obtained for the C4–C12 based devices, respectively. The charge transfer resistance decreased with increasing alkyl chain length. These results

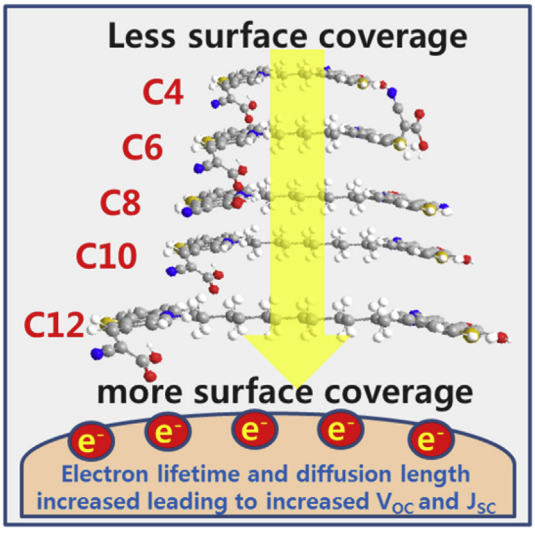

Fig. 9. Schematic adsorption coverage for the dyes C4–C12.

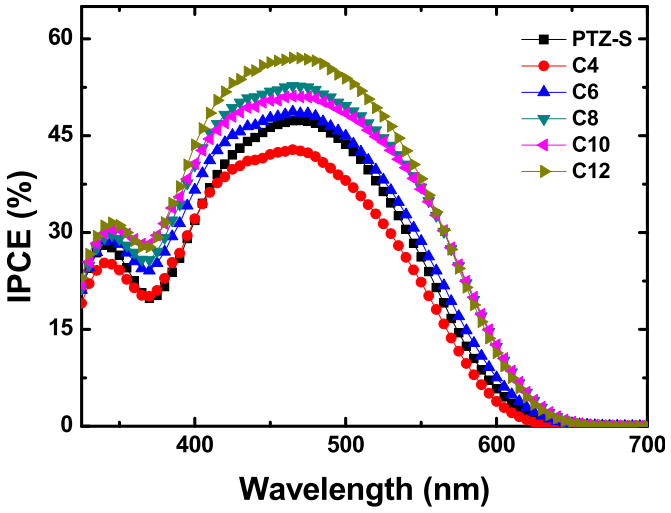

Fig. 10. IPCE spectra of the DSSCs based on C4–C12 and PTZ-S.

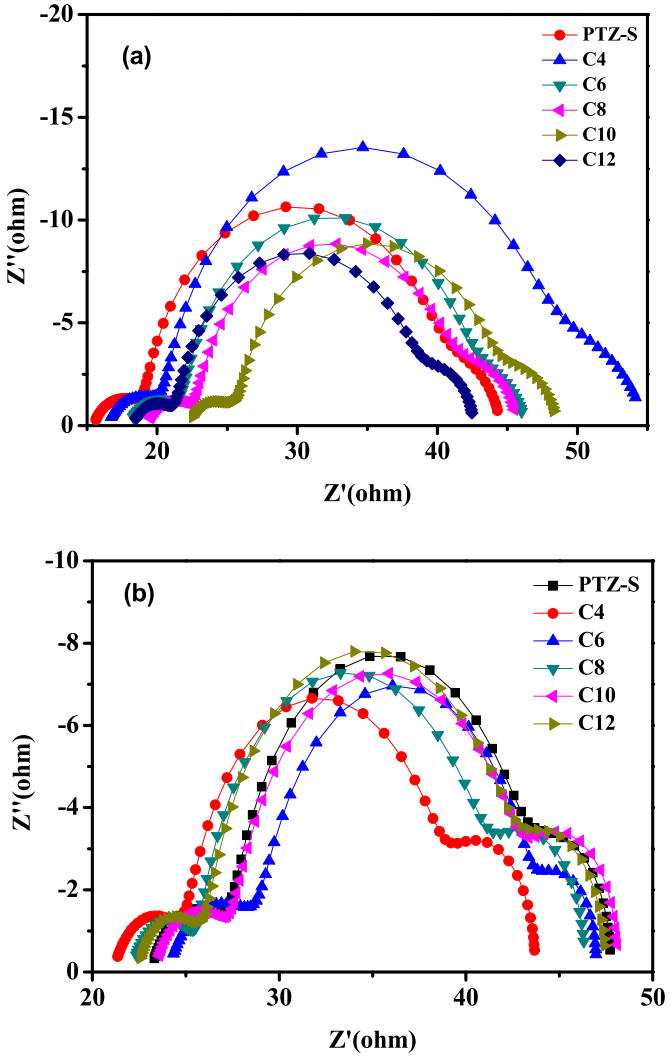

Fig. 11. Electrochemical impedance spectra (a) measured under illuminated condition (b) measured in the dark for DSSCs sensitized by C4–C12 and PTZ-S.

Table 3
EIS analysis of the DSSCs under illumination and dark conditions.

Dye	Illumination			Dark		
	R1	R2	R3	R1	R2	R3
PTZ-S	18.82	4.312	22.48	23.14	4.415	14.78
C4	16.44	3.818	24.91	21.13	3.946	12.83
C6	18.01	3.872	19.48	24.06	5.132	13.78
C8	19.28	3.429	17.38	22.13	3.531	14.56
C10	22.23	3.599	17.30	23.34	4.257	14.50
C12	18.26	3.133	16.37	22.37	3.727	15.71

show that an increase in the alkyl chain length is beneficial for improving the charge transfer process, resulting in a larger J_{SC} value. To further understand the electron recombination in DSSCs, EIS was carried out under dark conditions. Fig. 11b shows the Nyquist plots for the DSSCs based on the dyes, and Table 3 lists the corresponding parameters. Under dark impedance analysis, recombination resistance (R3) values of 12.83, 13.78, 14.56, 14.50, and 15.71 Ω were obtained for the C4–C12-based devices, respectively. Increasing the alkyl chain length is beneficial for restricting electron recombination, resulting in a larger recombination resistance. This suggests that the recombination of injected electron with an oxidized electrolyte can be suppressed more effectively by introducing long alkyl chains to the double donor-acceptor dyes.

To determine which parameters influence the device performance according to the length of alkyl chain, stepped light-induced transient measurements of the photocurrent and voltage (SLIM-PCV) measurements are conducted. This method has a simpler set-up and shorter measurement time compared to the pulsed-laser-induced current transients and intensity-modulated photovoltage spectroscopy [31,57,58]. A HeNe laser is used as the excitation source and white light with different irradiance are applied at various light biases. Their light irradiance was controlled by changing the ND filter prior to irradiation of each sample. The photocurrent and voltage decay with the excitation laser is chopped. Their decay can be fitted to the exponential decay function. Fig. 12a gives an example of photocurrent decay, which was measured using the ND filter with an optical density (OD) of 2.0. The photocurrent decay can be fitted using the following function [57]:

$$J_{SC}(t) = \beta \times e^{-t/\tau_c}$$

where J_{SC} (t), β, and τ_c are the photo-current decay, weight parameter and the time constant. Using the fitted constant of τ_c, D_e can be obtained from the following equation [57]:

$$D_e = \frac{L^2}{2.77\tau_c}$$

where L_e is the thickness of the electrode. Table 4 present the electron diffusion coefficient in each DSSC according to the stationary J_{SC} controlled by changing the light irradiance. The electron diffusion coefficient, which is calculated by fitting the curve at Fig. 12a, tends to increase with increasing alkyl chain length indicating that the electron can travel more through the TiO_2 matrix in the case of long alkyl chain containing devices. In particular, the C10 and C12-based devices accelerates charge transfer from TiO_2 to the current collector.

Similarly, time-resolved photo-voltage measurements using a HeNe laser as the excitation source are conducted to estimate the lifetime of photo-generated electron. The chopper was used to cut the excitation, and the decay of photo-voltage was measured using an oscilloscope. Fig. 12b gives an example of photo-voltage decay,

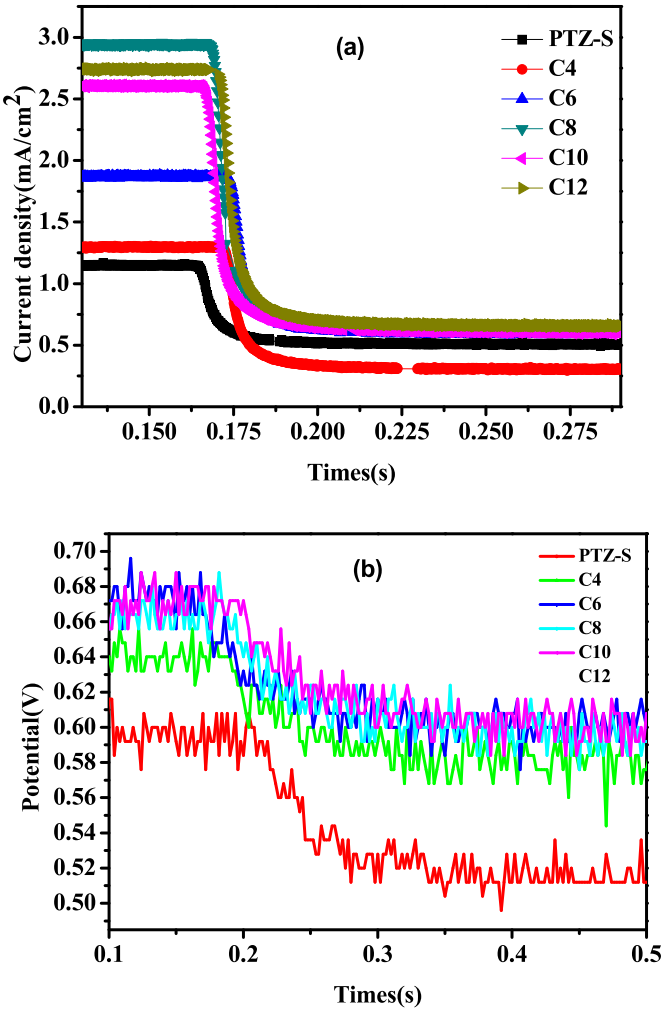

Fig. 12. (a) Typical current responses of the DSSCs against the different stepped laser intensities; (b) typical open circuit voltage transients induced by the stepped laser intensity.

Table 4
SLIM-PCV analysis of C4–C12 and PTZ-S.

Dye	D_e($cm^2/s \times 10^{-5}$)	τ_e(s)	L_e(μm)
PTZ-S	4.548	0.0519	15.37
C4	3.794	0.0517	14.00
C6	4.247	0.0567	15.52
C8	4.593	0.0594	16.52
C10	4.715	0.0628	17.21
C12	4.905	0.0662	18.01

which was measured using the ND filter with an OD of 2.0. The lifetime of a photo-generated electron can be estimated by fitting with the theoretical exponential equation, as follows [57]:

$$V_{oc}(t) = \alpha \times e^{-t/\tau_e}$$

where V_{OC} (t), α, and τ_e are the photo-voltage decay, weight parameter, and lifetime of the photo-generated electron, respectively. The electron lifetime, which is calculated by fitting the curves in Fig. 12b shows how much time an electron spends in the TiO_2 film before recombination. The electron lifetime increased with increasing alkyl chain length, which further supports the fact that there is marked suppression in recombination as the chain

length is changed from C4–C12. This suppression in recombination would lead to a decrease in dark current, leading to a high Voc. Finally, the electron diffusion length (L_e) is a useful tool for reflecting the electron collection efficiency (η_c) and it can be estimated as follows [57]:

$$L_e = \sqrt{D_e \times \tau_e}$$

Similar to the case of D_e, the L_e (Table 4) tends to increase with increasing alkyl chain length and C10 and C12 shows the longer diffusion lengths among the samples tested. The longer L_e of C10 and C12 can be attributed mainly to the high diffusion coefficient. As the L_e increases, the likelihood of charge separation at the TCO surface increases, leading to higher electron collection efficiency. Therefore, more photo-generated electrons can move to the current collector with a higher L_e, resulting in significant enhancement of the photovoltaic performance.

4. Conclusion

A series of double donor-acceptor organic dyes bridged by different alkyl chain spacers were synthesized and examined for DSSC applications. The results suggest that increasing the alkyl chain length has a significant effect on the physical and electrochemical properties, and when the dyes are applied to DSSCs, Jsc and the maximum IPCE of the devices increase gradually with increasing alkyl chain length. The long alkyl chains provide an efficient shielding effect to retard charge recombination, and resulting in an improvement of the V_{OC}. EIS showed that an increase in the alkyl chain length could suppress the charge transfer resistance/charge recombination between the injected electrons with oxidized species. Furthermore, the electron lifetime and diffusion parameters estimated by SLIM-PCV studies show that there is a marked increase in the overall performance of the devices as the alkyl chain length in the dye molecule increases. This could be due to the improved charge transfer, electron lifetime and diffusion length as well as to the decreased recombination resistance, which leads to the rapid regeneration of the sensitizing dye. In case of the C4 dye, the charge transfer resistance increased and the diffusion length decreased, rendering a decrease in overall efficiency. Therefore, the device with the dye molecule containing a longer alkyl chain length showed good conversion efficiency of the DSSC. This work systematically investigated the influence of the alkyl chain length on the photovoltaic performance of DSSCs, which will pave the way for further improvements in double donor-acceptor organic dyes.

Acknowledgements

This study was supported by the New & Renewable Energy Core Technology Program of the Korea Institute of Energy Technology Evaluation and Planning (KETEP) granted financial resource from the Ministry of Trade, Industry & Energy, Republic of Korea (No. 20133010011750). J.J. wishes to thank the Korea Institute of Science and Technology Information for the use of the PLSI supercomputing resources.

Appendix A. Supplementary data

Supplementary data related to this article can be found at http://dx.doi.org/10.1016/j.dyepig.2016.05.035

References

[1] Mishra A, Markus K, Fischer R, Bauerle P. Metal-free organic dyes for dye-sensitized solar cells:from structure property relationships to design rules. Angew Chem Int Ed 2009;48(14):2474–99.
[2] Wu Y, Zhu W. Organic sensitizers from D-π-A to D-A-π-A: effect of the internal electron-withdrawing units on molecular absorption, energy levels and photovoltaic performances. Chem Soc Rev 2013;42(5):2039–58.
[3] Chuan-Pei L, Ryan Yeh-Yung L, Lu-Yin L, Chun-Ting L, Te-Chun C, Shih-Sheng S, et al. Recent progress in organic sensitizers for dye-sensitized solar cells. RSC Adv 2015;5(30):23810–25.
[4] Hagberg DP, Yum JH, Lee HJ, De Angelis F, Marinado T, Karlsson KM. Molecular engineering of organic sensitizers for dye-sensitized solar cell applications. J Am Chem Soc 2008;130(19):6259–66.
[5] Ooyama Y, Harima Y. Molecular designs and syntheses of organic dyes for dye-sensitized solar cells. Eur J Org Chem 2009;2009(18):2903–34.
[6] Clifford JN, Planells M, Palomares E. Advances in high efficiency dye sensitized solar cells based on Ru(II) free sensitizers and a liquid redox electrolyte. J Mater Chem 2012;22(46):24195–201.
[7] Chen Z, Li F, Huang C. Organic D-pi-A dyes for dye-sensitized solar cell. Curr Org Chem 2007;11(14):1241–58.
[8] Fischer MKR, Wenger S, Wang MK, Mishra A, Grätzel M. D-p-A sensitizers for dye-sensitized solar cells: linear vs branched oligothiophenes. Chem Mater 2010;22(5):1836–45.
[9] Yen YS, Chou HH, Chen YC, Hsu CY, Lin JT. Recent developments in molecule-based organic materials for dye-sensitized solar cells. J Mater Chem 2012;22(18):8734–47.
[10] Kang X, Zhang J, O'Neil D, Rojas AJ, Chen W, Szymanski P, et al. Effect of molecular structure perturbations on the performance of the D-A-π-A dye sensitized solar cells. Chem Mater 2014;26(15):4486–93.
[11] Yang J, Ganesan P, Teuscher J, Moehl T, Tian H, Grätzel M, et al. Influence of the donor size in D-π-A organic dyes for dye-sensitized solar cells. J Am Chem Soc 2014;136(15):5722–30.
[12] Hua Y, Chang S, Chen T, Wong WY, Wong WK. Significant improvement of dye-sensitized solar cell performance using simple phenothiazine-based dyes. Chem Mater 2013;25(10):2146–53.
[13] Feng Q, Zhou G, Wang ZS. Varied alkyl chain functionalized organic dyes for efficient dye-sensitized solar cells: influence of alkyl substituent type on photovoltaic properties. J Power Sources 2013;239:16–23.
[14] Zhang M, Wang Y, Ma W, Li R, Wang P. Design of high-efficiency organic dyes for titania solar cells based on the chromophoric core of cylopentadithiophene-benzothiadizole. Energy Environ Sci 2013;6(10):2944–9.
[15] Kim BG, Chung K, Kim J. Molecular design principle of all-organic dyes for dye-sensitized solar cells. Chem Eur J 2013;19(17):5220–30.
[16] Zeng W, Cao Y, Bai Y, Wang Y, Pan C, Wang P. Efficient dye-sensitized solar cells with an organic photosensitizer featuring orderly conjugated ethylenedioxythiophene and dithienosilole blocks. Chem Mater 2010;22(5):1915–25.
[17] Hara K, Sayama K, Arakawa H, Ohga Y, Shinpo Am. A coumarin-derivative dye sensitized nanocrystalline TiO_2 solar cell having a high solar-energy conversion efficiency up to 5.6%. Chem Commun 2001;6:569–70.
[18] Derong C, Jinan P, Yanping H, Xiaoming F, Herbert M. Enhanced performance of the dye-sensitized solar cells with phenothiazine-based dyes containing double D-A branches. Org Lett 2011;13(7):1610–3.
[19] Yanping H, Dai-Bin K, Lingyun W, Herbert M, Cheng-Yong S. Organic dye bearing asymmetric double donor-n-acceptor chains for dye-sensitized solar cells. J Org Chem 2011;76(19):8015–21.
[20] Yanping H, Dai-Bin K, Herbert M, Cheng-Yong S, Derong C. Performance of dye-sensitized solar cells based on novel sensitizers bearing asymmetric double D-n-A chains with arylamines as donors. Dyes Pigments 2012;94:481–9.
[21] Xu-Feng Z, Teng-Long Z, Zu-Sheng H, Zafar I, Derong C. Impact of the position isomer of the linkage in the double D-A branch-based organic dyes on the photovoltaic performance. Dyes Pigments 2014;104:89–96.
[22] Zu-Sheng H, Cheng C, Xu-Feng Z, Zafar I, Derong C. Effect of the linkage location in double branched organic dyes on the photovoltaic performance of DSSCs. J Mater Chem A 2015;3(3):1333–44.
[23] Ren X, Jiang S, Cha M, Zhou G, Wang ZS. Thiophene-bridged double D-π-A dye for efficient dye-sensitized solar cell. Chem Mater 2012;24(17):3493–9.
[24] Tian H, Yang X, Chen R, Pan Y, Hagfeldt A, Sun L, et al. Phenothiazine derivatives for efficient organic dye-sensitized solar cells. Chem Commun 2007;36:3741–3.
[25] Wang S, Wang H, Guo J, Tang H, Zhao J. Influence of the terminal electron donor in D–D–π–A phenothiazine dyes for dye-sensitized solar cells. Dyes Pigments 2014;109:96–104.
[26] Gang W, Yingying W, Wenhui D, Guipeng Y, Yingping Z, Chunyue P, et al. Photovoltaic performance of long-chain poly(triphenylamine-phenothiazine) dyes with a tunable pi-bridge for dye-sensitized solar cells. J Mater Chem A 2015;3(27):14217–27.
[27] Hailang J, Kang S, Xuehai J, Mingdao Z, Hegen Z. Enhanced performance of dye-sensitized solar cells with Y-shaped organic dyes containing di-anchoring groups. New J Chem 2016;40(3):2799–805.
[28] Wei-I H, You-Ya L, Ting-Hui L, Yu-Chien T, Tzu-Chien W, Yung-Sheng Y. Eugenic metal-free sensitizers with double anchors for high performance dye-sensitized solar cells. Chem Commun 2015;51(51):2152–5.
[29] Wei-I H, You-Ya L, Chih-Yu H, Hsien-Hsin C, Wei-Siang K, Jiann TL. High-Performance dye-sensitized solar cells based on phenothiazine dyes containing double anchors and thiophene spacers. Chem Asian J 2014;9(1):

357–66.
[30] Kim MS, Cho MJ, Choi YC, Kim K, Kim JH. Enhancement of photovoltaic performance in dye-sensitized solar cells fabricated with dendritic photosensitizer containing site-isolated chromophores. Dyes Pigments 2013;99(3):986–94.
[31] Park JH, Jang BY, Thogiti S, Ryu J-H, Kim S-H, Son Y-A, et al. A comparison of the optical and photovoltaic properties of novel double branched organic dyes in dye sensitized solar cells. Synth Met 2015;203:235–42.
[32] Koumura N, Wang ZS, Shogo M, Suzuki E, Hara K. Alkyl-functionalized organic dyes for efficient molecular photovoltaics. J Am Chem Soc 2006;128(44):14256–7.
[33] Kroeze JE, Hirata N, Schmidt-Mende L, Grätzel M, Durrant JR. Alkyl chain barriers for kinetic optimization in dye-sensitized solar cells. J Am Chem Soc 2006;128(50):16376–83.
[34] Clara B, Stefania B, Emanuela L, Paola M, Norberto M, Alessandro A. Benzodithiophene based organic dyes for DSSC: effect of alkyl chain substitution on dye efficiency. Dyes Pigments 2015;121:351–62.
[35] Zhongquan W, Chunyang J, Yan W, Xiaojun Y. Dithiafulvenyl–triphenylamine organic dyes with alkyl chains for efficient coadsorbent-free dye-sensitized solar cells. RSC Adv 2015;5(63):50813–20.
[36] Mathew S, Iijima H, Toude Y, Ito S, Imahori H. Optical, electrochemical and photovoltaic effects of an electron-withdrawing tetrafluorophenylene bridge in a push-pull porphyrin sensitizer used for dye-sensitized solar cells. J Phys Chem C 2011;115(29):14415–24.
[37] Ripolles-Sanchis T, Pan TS, Lee HW, Raga SR, WDiau E. Design and characterization of alkoxy-wrapped push-pull porphyrins for dye-sensitized solar cells. Chem Commun 2012;48(36):4368–70.
[38] Kang SH, Ju MJ, Hong JY, Kang HS, Kim HK. Novel D-n-A Structured porphyrin dyes with diphenylamine derived electron-donating substituents for highly efficient dye-sensitized cells. J Mater Chem A 2013;1(12):3977–82.
[39] Xiaodong X, Weihong Z, Nuonuo Z, Yaqing F, Bao Z. Effect of the length of the alkyl chains in porphyrin meso-substituents on the performance of dye-sensitized solar cells. RSC Adv 2014;4(17):8894–900.
[40] Hu X, Cai S, Tian G, Li X, Su J, Li J. Rigid triarylamine-based D-A-π-A structural organic sensitizers for solar cells: the significant enhancement of open-circuit photovoltage with a long alkyl group. RSC Adv 2013;3(44):22544–53.
[41] Kim MS, Yang HS, Jung DY, Han YS, Kim JH. Effects of the number of chromophores and the bulkiness of a nonconjugated spacer in a dye molecule on the performance of dye-sensitized solar cells. Coll Surf A 2013;420:22–9.
[42] Won YS, Kim JH, Ryu J-H, Kim KK, Park SS. Organic photosensitizers based on terthiophene with alkyl chain and double acceptors for application in dye-sensitized solar cells. Energy Fuels 2010;24(6):3676–81.
[43] Qipeng C, Wenqin L, Yongzhen W, Kai P, Weihong Z. Effect of a long alkyl group on cyclopentadithiophene as a conjugated bridge for D–A–π–A organic sensitizers: IPCE, electron diffusion length, and charge recombination. ACS Appl Mater Interfaces 2014;6(16):14621–30.
[44] Lu X, Jia X, Wang Z, Zhou G. X-shaped organic dyes with a quinoxaline bridge for use in dye-sensitized solar cells. J Mater Chem A 2013;1(34):9697–706.
[45] Gao P, Tsao HN, Grätzel M, Nazeeruddin MK. Fine-tuning the electronic structure of organic dyes for dye-sensitized solar cells. Org Lett 2012;14(17):4330–3.
[46] Haid S, Marszalek M, Mishra A, Wielopolski M, Bauerle P. Significant improvement of dye-sensitized solar cell performance by small structural modification in π-conjugated donor–acceptor dyes. Adv Funct Mater 2012;22(6):1291–302.
[47] Frisch MJ, Trucks GW, Schlegel HB, Scuseria GE, Cioslowski J, Fox DJ, et al. Wallingford CT. 2009.
[48] Becke AD. Density-functional thermochemistry. III. The role of exact exchange. J Chem Phys 1993;98(7):5648–52.
[49] Becke AD. Density-functional thermochemistry. IV. A new dynamic correlation functional and implications for exact-exchange mixing. J Chem Phys 1996;104(3):1040–6.
[50] Lee C, Yang W, Parr RG. Development of the Colle-Salvetti correlation-energy formula into a functional of the electron density. Phys Rev B Condens Matter 1988;37(2):785–9.
[51] Yanai T, Tew DP, Handy NC. A new hybrid exchange-correlation functional using the Coulomb-attenuating method (CAM-B3LYP). Chem Phys Lett 2004;393(1–3):51–7.
[52] Miertuš S, Scrocco E, Tomasi J. Electrostatic interaction of a solute with a continuum. A direct utilization of ab initio molecular potentials for the prevision of solvent effects. J Chem Phys 1981;55(1):117–29.
[53] Cossi M, Barone V, Cammi R, Tomasi J. Ab initio study of solvated molecules: a new implementation of the polarizable continuum model. Chem Phys Lett 1996;255(4–6):327–35.
[54] Sagakuchi S, Pandey SS, Okada K, Yamaguchi Y, Hayase S. Probing TiO_2/Dye interface in dye sensitized solar cells using surface potential measurement. Appl Phys Express 2008;1(10):105001–3.
[55] Pandey SS, Sakakushi S, Yamaguchi Y, Hayase S. Influence of nature of surface dipoles on observed photovoltage in dye-sensitized solar cells as probed by surface potential measurement. Org Electron 2010;11(3):419–26.
[56] Jinwei L, Weihe X, Yong S. TiO2 nanofiber based dye sensitized solar cells with improved carrier collection efficiency. Trans Control Mech Syst 2012;1(6):235–8.
[57] Nakade S, Kanzaki T, Wada Y, Yanagida S. Stepped light-induced transient measurements of photocurrent and voltage in dye-sensitized solar cells: application for highly viscous electrolyte systems. Langmuir 2005;21(23):10803–7.
[58] Nguyen TH, Suresh T, Kim JH. Dye mixture promoted light harvesting for organic dye-sensitized solar cells using triphenylamine dyes with various numbers of anchoring groups. Org Electron 2016;30:40–4.